# SANDIA REPORT

SAND2003-4112
Unlimited Release
Printed November 2003

# Numerical Predictions and Experimental Results of a Dry Bay Fire Environment

Amalia Black, Walt Gill, and Jill Suo-Anttila

Prepared by
Sandia National Laboratories
Albuquerque, New Mexico 87185 and Livermore, California 94550

Sandia is a multiprogram laboratory operated by Sandia Corporation,
a Lockheed Martin Company, for the United States Department of Energy's
National Nuclear Security Administration under Contract DE-AC04-94AL85000.



Issued by Sandia National Laboratories, operated for the United States Department of Energy by Sandia Corporation.



Available to DOE and DOE contractors from
U.S. Department of Energy
Office of Scientific and Technical Information
P.O. Box 62
Oak Ridge, TN 37831

Telephone: (865)576-8401
Facsimile: (865)576-5728
E-Mail: reports@adonis.osti.gov
Online ordering: http://www.doe.gov/bridge

Available to the public from
U.S. Department of Commerce
National Technical Information Service
5285 Port Royal Rd
Springfield, VA 22161

Telephone: (800)553-6847
Facsimile: (703)605-6900
E-Mail: orders@ntis.fedworld.gov
Online order: http://www.ntis.gov/help/ordermethods.asp?loc=7-4-0#online

SAND2003-4112
Unlimited Release
Printed November 2003

# Numerical Predictions and Experimental Results of a Dry Bay Fire Environment

Amalia Black
Validation and Uncertainty Quantification Processes

Walt Gill and Jill Suo-Anttila
Fire Science and Technology

Sandia National Laboratories
P.O. Box 5800
Albuquerque, NM 87185

## Abstract

The primary objective of the Safety and Survivability of Aircraft Initiative is to improve the safety and survivability of systems by using validated computational models to predict the hazard posed by a fire. To meet this need, computational model predictions and experimental data have been obtained to provide insight into the thermal environment inside an aircraft dry bay. The calculations were performed using the Vulcan fire code, and the experiments were completed using a specially designed full-scale fixture. The focus of this report is to present comparisons of the Vulcan results with experimental data for a selected test scenario and to assess the capability of the Vulcan fire field model to accurately predict dry bay fire scenarios. Also included is an assessment of the sensitivity of the fire model predictions to boundary condition distribution and grid resolution. To facilitate the comparison with experimental results, a brief description of the dry bay fire test fixture and a detailed specification of the geometry and boundary conditions are included. Overall, the Vulcan fire field model has shown the capability to predict the thermal hazard posed by a sustained pool fire within a dry bay compartment of an aircraft; although, more extensive experimental data and rigorous comparison are required for model validation.

## Acknowledgements

This work was sponsored by the OSD/DOT&E, LFT&E office under the Safety and Survivability of Aircraft Initiative. The authors would like to acknowledge James O'Bryon and Juan Vitali for management and sponsorship of this effort.

## Table of Contents


**1. INTRODUCTION ..... 7**

**2. EXPERIMENTAL APPROACH ..... 9**

2.1 TEST FIXTURE DESCRIPTION ..... 9
2.2 INSTRUMENTATION DESCRIPTION ..... 11

**3. NUMERICAL MODELING ..... 13**

**4. GRID GENERATION ..... 14**

**5. BOUNDARY CONDITIONS ..... 15**

5.1 AIR INLET ..... 15
5.2 FUEL INLET ..... 16
5.3 OUTLET ..... 17
5.4 WALLS ..... 17

**6. SIMULATION MATRIX ..... 18**

**7. RESULTS ..... 19**

7.1 VULCAN PREDICTIONS AND EXPERIMENTAL COMPARISONS ..... 19
7.2 SENSITIVITY CALCULATIONS ..... 22

**8. CONCLUSIONS ..... 25**

**REFERENCES ..... 27**

**DISTRIBUTION ..... 28**

# List of Figures

FIGURE 1 – DRY BAY SIMULATOR PHOTOGRAPH ..... 9
FIGURE 2 – SCHEMATIC OF THE DRY BAY FIRE SIMULATOR ..... 10
FIGURE 3 – THE AIRFLOW SYSTEM FOR THE DRY BAY SIMULATOR ..... 11
FIGURE 4 – SECTION OF FINE COMPUTATIONAL GRID ..... 14
FIGURE 5 – INLET AIR VELOCITY AND TURBULENCE INTENSITY DISTRIBUTION ..... 16
FIGURE 6 – FUEL VELOCITY AND TURBULENCE INTENSITY DISTRIBUTION ..... 17
FIGURE 7 – PREDICTED GAS TEMPERATURES AND THERMOCOUPLE VALUES ..... 20
FIGURE 8 – PREDICTED HEAT FLUX DISTRIBUTION AND MEASURED VALUES ..... 20
FIGURE 9 – SOLUTION SENSITIVITY TO GRID SIZE ..... 22
FIGURE 10 – PREDICTED TEMPERATURE DISTRIBUTION FOR VARIOUS INLET CONDITIONS 23
FIGURE 11 – PREDICTED HEAT FLUX DISTRIBUTION FOR VARIOUS INLET CONDITIONS .... 24

# 1. Introduction

Damage to Department of Defense (DoD) aircraft from blast and fire causes excessive loss of life and property. Due to the highly complex nonlinear nature of fires and explosions, efforts to reduce these losses have been addressed previously, as best as possible, with a large number of costly tests. In recognition of the technical and economic limitations of the present approach, the Live Fire Test and Evaluation (LFT&E) office of the Director of Operational Test and Evaluation (DOT&E) created the Safety and Survivability of Aircraft Initiative (SSAI).

As part of the SSAI program, efforts are being devoted within the DoD and at Sandia National Laboratories (SNL) to yield major improvements in fire safety under all system operating conditions, including improvements in fire survivability of systems subjected to hostile fire. These safety and survivability improvements will be obtained through the use of validated computational models developed to predict the hazard posed by the fire as well as the effectiveness of fire suppression strategies. Although the value of modeling and simulation is widely recognized, the development of credible models poses significant technical challenges because the individual and interaction between relevant physical mechanisms to be represented by these models is complex.

Prediction of the fire environment inside an aircraft dry bay can be made using either engineering models or physics-based fire field models. Confidence in using modeling and simulation must be gained through comparison with data, i.e., model validation. For proper validation, a thorough assessment of the model utility should be obtained using data collected specifically for the scenario of interest. Although data from enclosed fires exists, the scenarios documented are either not directly applicable to dry bay fires or necessary detailed data has not been acquired to be suitable for model validation. For this reason, experiments were conducted in the specially designed dry bay simulator at Wright Patterson Air Force Base [1]. Pre-test calculations of a dry bay fire were performed to assist in the design and execution of the experiments [2].

In the present study, model predictions were compared to data collected using the dry bay fire simulator. This comparison provided an assessment of the potential of the fire model to predict the thermal hazard resulting from a dry bay fire in a live fire test or hostile fire scenario. This report 1) presents predictions of a dry bay fire environment, 2) assesses the

sensitivity of the model predictions to changes in the boundary conditions, 3) compares the model predictions to an experimental data set, and 4) assesses the performance of the Vulcan fire field model in predicting the outcome of actual dry bay fires.

# 2. Experimental Approach

A primary objective of the experiments was to provide insight into the physical mechanisms of a dry bay fire and to collect data for comparison with fire model predictions. A dry bay fire simulator, which possesses realistic features and allows for accurate control of important parameters (i.e. ventilation flow rate, ventilation location, fuel flow rate, and fuel release location), was designed for use in the experiments. The test fixture also contains ample diagnostics for measurement of thermal response; therefore, the facility is suitable for providing high quality validation data.

## 2.1 Test Fixture Description

The basic dry bay simulator hardware configuration was selected based on a preliminary assessment of model predictions [2]. A rectangular duct, with an air inlet at one end and an outlet at the other, was constructed. Figure 1 is a photograph of the test fixture. The test fixture is constructed of Titanium alloy 6 Al - 4 V and is approximately 1.5 x 0.3 x 0.8 m overall in size. A schematic showing the internal dimensions of the dry bay simulator is shown in Figure 2. In that figure, it can be seen that the duct is composed of an upstream test section and a downstream mixing box section. The air inlet location of the test section can be positioned either at the top or the bottom of the front wall. The exit location of the test section is always in the center of the rear wall of the section. A more detailed description of the dry bay simulator can be found in Gill, et al. [1].

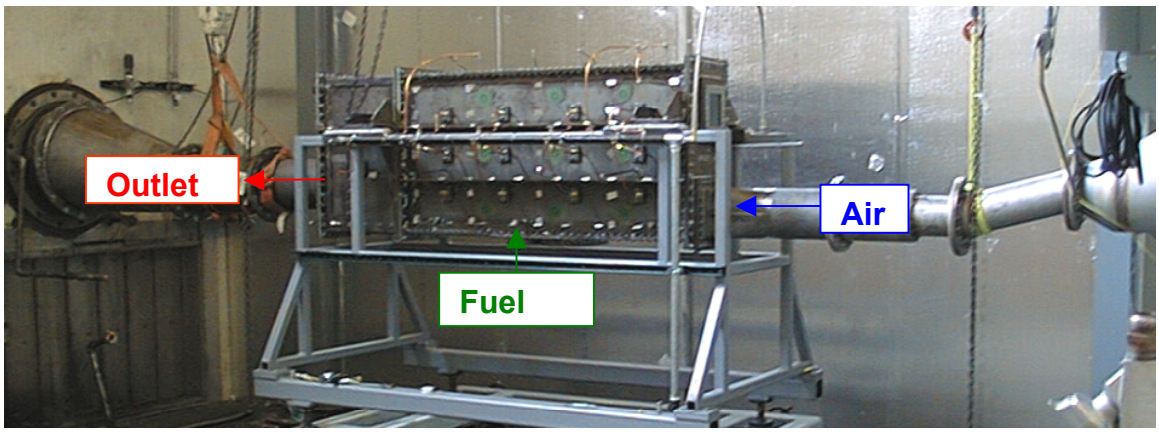


**Figure 1 – Dry Bay Simulator Photograph**

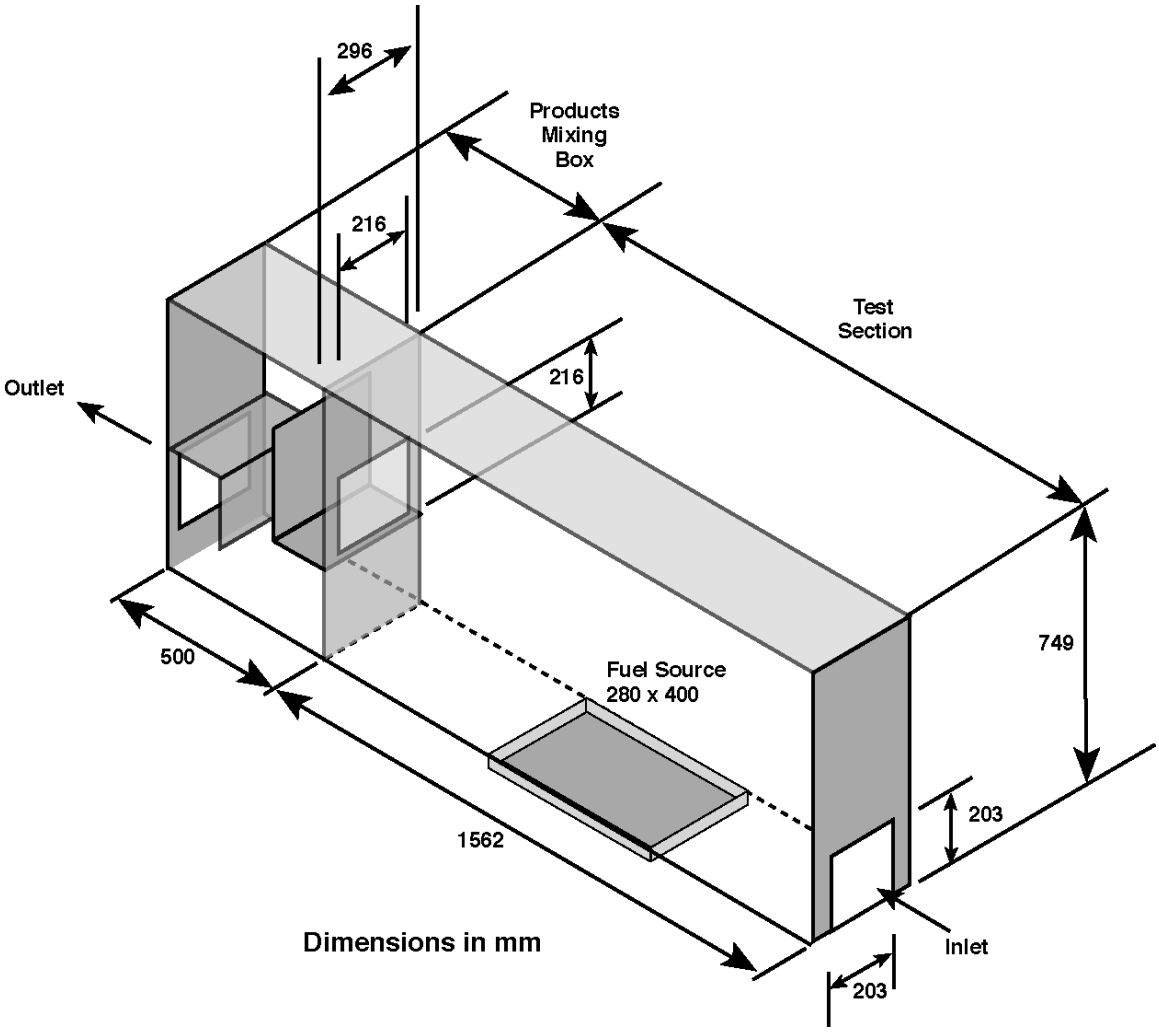


**Figure 2 – Schematic of the Dry Bay Fire Simulator**

A moveable fuel source is provided in the floor of the test section that can either be a pool of liquid or a gas flow (methane in this study) through a porous plate. The gaseous (methane) fuel system is composed of a large volume high-pressure supply reservoir connected to the fuel bed via a sonic orifice flow control device. The upstream pressure on the orifice is controlled with a two-stage regulator that is set to a value determined by the desired the gas temperature and flow rate. The porous plate through which the methane gas flow passes as it enters into the dry bay is formed from a 3 mm thick stainless steel "felt metal" material.

The airflow into and out of the dry bay is controlled via an air ejector fitted to the duct exit and a throttle at the inlet. Figure 3 shows the air supply system for the test facility. The setup is an ejector actuated pull-through system with inlet air metering on inlet side. The ejector draws ambient air from laboratory through the test set up. By adjusting the various valves in the system, it is possible to maintain different combinations of duct airflow (inlet velocity) and duct pressure. Facilities for injecting flame suppressant and cooling gas are present for thermal protection of the pollution control equipment on the exhaust side.

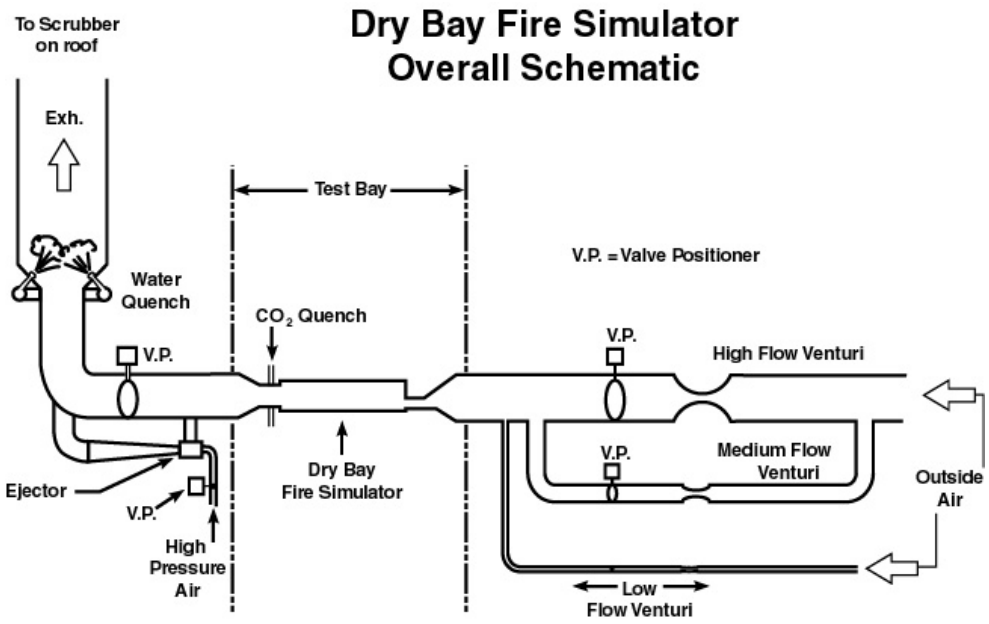


**Figure 3 – The Airflow System for the Dry Bay Simulator**

## 2.2 Instrumentation Description

Instrumentation included thermocouples, heat flux gauges on the duct walls, and video cameras. The thermocouple instrumentation includes thermocouple arrays in the flow and on the duct wall. The flow thermocouples are 1.6 mm diameter type S sheathed thermocouple (TC) assemblies. There are a total of 65 TCs that form 3-instrumented planes in the duct. An axial plane of symmetry is formed from an array of 25 TCs positioned vertically along the centerline of the duct. A cross-sectional plane at the duct center is formed from 20 additional TCs. A second cross-sectional plane at the inlet end is formed from the remaining 20 TCs. The cross-sectional arrays can be moved

to other locations along the length of the duct. It is acknowledged that, due to several mechanisms, including radiative transport and thermal inertia, the temperature measured using a thermocouple is not, in general, equal to the local gas temperature. Cost and robustness limitations, however, continue to dictate the use of thermocouples for the spatial characterization of fires. The difference in thermocouple temperatures should not be considered an error but rather a response of an instrument to the fire environment. In order to make a direct comparison, models of the thermocouple should be included in the fire code.

The heat flux gages on the duct walls are made from thermocouple arrays. Type K thermocouple wires are welded to form intrinsic junctions on the outer surface of the wall in specially prepared locations. Each instrumented location is a thermally isolated disk formed from the wall material by means of a deep groove cut. The thermocouple time history is used in conjunction with an energy balance equation of the disk which allows the calculation of the net heat flux from the duct interior to the inside surface of the wall.

Lastly, three video cameras were positioned adjacent to the window on the inlet wall, providing views of the pool, the centerline of duct, and the upper regions of duct.

The dry bay fire simulator was used in a series of tests designed to investigate the fire environment under varying conditions. A large database was created by systematically varying fuel and air inlet flow rates and locations. A single test, for which a complete set of boundary conditions were measured, was selected for detailed comparison with model predictions. For this test, the simulator was configured with the inlet in the upper portion of the duct. Methane fuel was used and introduced through a fuel source that was centered along the bottom wall of the test section.

Three repeatability tests were conducted to investigate the experimental variability. In comparing the 3 baseline tests, the thermocouple readings from 95 to 105 seconds were within 5% of reading for TC's below 800K and within 4% of reading for TC's above 800K. Thus, the average standard deviation in observed temperatures is +/-5% of the reading. In addition, the heat flux data also showed a +/-5% uncertainty based on an analysis of the heat flux instrumentation. Further details on the uncertainty calculations can be found in the experimental data report (Gill, et al.).

# 3. Numerical Modeling

The computational modeling portion of this effort was performed using the Vulcan fire field model. Vulcan has been developed over the past 8 years at Sandia National Laboratories (SNL) in collaboration with the SINTEF Foundation and the Norwegian University of Science and Technology (NUST). Vulcan is derived from the KAMELEON fire model and uses an extension of the SIMPLEC method of Patankar and Spalding [3] to solve the conservation equations on a structured, staggered, three-dimensional Cartesian finite difference grid. The "brick" mesh is employed in part to facilitate rapid solutions of participating media radiative heat transfer. The ability to resolve the geometry of the system is only limited by the ability to construct the appropriate grid with the Cartesian grid generator available in Vulcan. First- and second-order accurate upwind schemes can be used for the convective terms. Turbulence is modeled using a standard two equation k-ε model.

The combustion model in Vulcan is based on Magnussen's Eddy Dissipation Concept [4, 5]. The Eddy Dissipation Concept (EDC) is a general concept for describing non-premixed, mixing rate limited combustion, such as that which occurs in fires. The EDC assumes that the combustion process occurs in the turbulent flame structures, which can be modeled as perfectly stirred reactors. Vulcan presently assumes that the combustion process is irreversible and occurs infinitely fast, i.e., it does not include finite rate chemistry. However, an extinction limit is included in the model. Local extinction is assumed to occur when the time scale for turbulent mixing is less than the chemical time scale.

The modeling of soot formation is based on a two-step process adapted by Magnussen [6] from the work of Tesner, et al. [7]. The first step treats the formation of radical nuclei, and the second step treats the formation of soot particles from the radical nuclei. Once soot is formed, the EDC model includes the combustion of the soot in the flame.

Convective and participating media radiative heat transfer is modeled to objects in the flow field. Thermal radiation of the combustion products (including soot) is modeled using the Discrete Transfer Method of Shah [8]. This technique is used primarily because it represents an acceptable compromise between computational speed and accuracy for most problems. The soot and combustion gases are treated as a gray gas with a total absorption and emission coefficient.

# 4. Grid Generation

The geometry used in the simulations was identical to the experimental geometry (Figures 1 and 2) described in the Experimental Approach section. An accurate representation of the experimental test fixture was possible with the Cartesian grid generator within the Vulcan Graphical User Interface. Figure 4 shows a cross-section of the computational grid along the centerline of the dry bay. In the X-direction, the grid was refined towards the air inlet. In the Z-direction, the grid was refined around the inlet and exit regions. The grid was also refined similarly in the Y-direction (not shown in this figure). This three-dimensional Cartesian grid consisted of 112 (X-direction) by 39 (Y-direction) by 76 (Z-direction) grid points for a total of 331,968 grid points in the simulation. A less-refined grid was also generated in order to determine the sensitivity of the solution to the grid size. This medium grid consisted of 87x37x68 points for a total of 218,892 grid points. Both solutions were run on a cluster of SGI Origin 2000 processors until a steady state solution was reached. The fine mesh solution required 3 weeks of computing time and the medium mesh required 2 weeks.

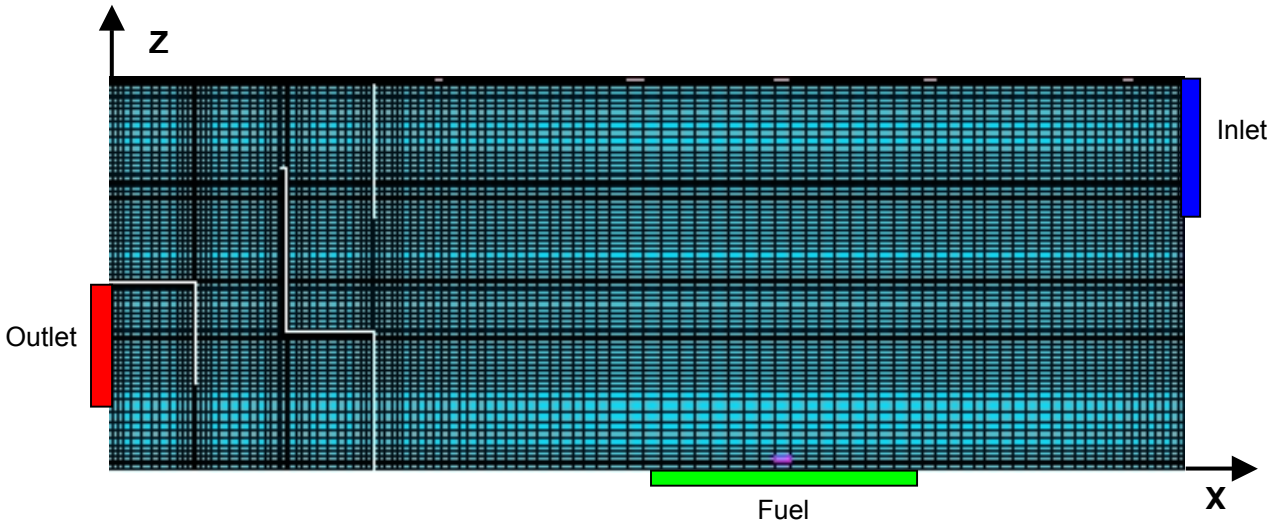


**Figure 4 – Section of Fine Computational Grid**

# 5. Boundary Conditions

In order to permit the experimental data to be compared to the numerical simulations, an accurate specification of the boundary conditions is required to perform the calculations. In the case of the dry bay simulator, the boundary conditions of interest occur at the air inlet, fuel inlet, and the outlet as shown in Figure 2. The outlet was specified as a constant pressure boundary condition. The characterization of the inlet and fuel boundary conditions is described in the sections below.

## 5.1 Air Inlet

The flow distribution in the air inlet was characterized in a series of non-reacting tests to quantify as best as possible the boundary conditions for the actual experiments. Due to limitations in supply air, a single run did not permit collection of all the data necessary to characterize the inlet. A total of four hot wire probes were simultaneously used to measure the velocity and turbulence intensity of the air entering the dry bay. The probes were traversed vertically; taking 21 data points each, across the inlet. The four probes were moved horizontally after each test and a total of five different runs were required to make measurements of the entire domain. Measurements were obtained at a total of 420 nodes in the air inlet.

The inlet air velocity distribution is shown in Figure 5. Note that the velocity in the upper portion of the duct is greater than the lower portion. The turbulence intensity measured at the inlet is also shown in Figure 5. The presented distribution contains enough detail to allow for accurate specification of the inlet air boundary condition in the computer simulation. The inlet velocity distribution presented in the figure was duplicated in the Vulcan simulation and the actual velocities were scaled to match the overall mass flow rate (0.1636 kg/sec). Allocated resources did not permit an assessment of the experimental variability, such as, conducting repeat boundary condition characterization experiments, to be performed.

Additional simulations were performed assuming uniform flow conditions at the air inlet. For these simulations, an average velocity is 4.205 m/s was used, which corresponds to the inlet mass flow rate measured in the experiment. From the average velocity value, the average turbulent kinetic energy was calculated assuming turbulent isotropic flow as follows:

$$k = \frac{\overline{u'^2} + \overline{v'^2} + \overline{w'^2}}{2} = \frac{3\overline{u'^2}}{2} = \frac{3(I\bar{u})^2}{2}$$

A value of 10% was assumed for the turbulence intensity, I.

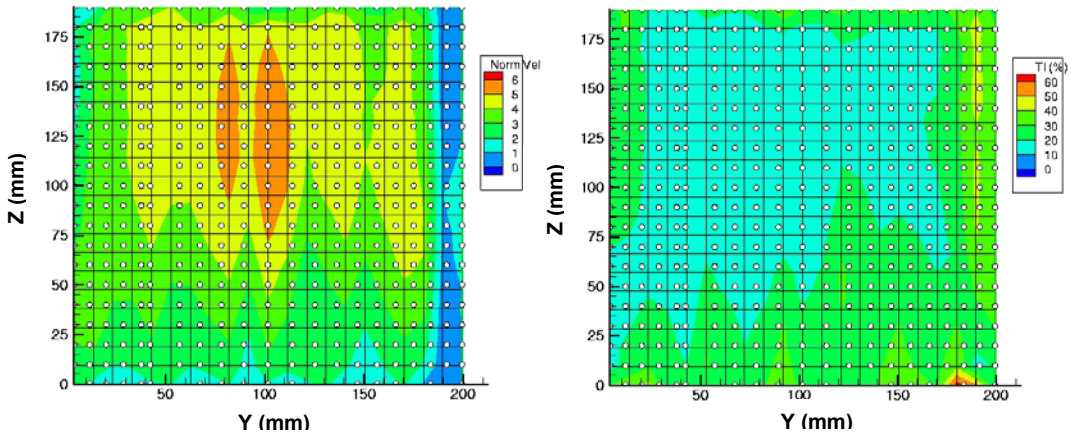


**Figure 5 – Inlet Air Velocity and Turbulence Intensity Distribution**

## 5.2 Fuel Inlet

The distribution of the fuel was characterized in a manner similar to the inlet air velocity. Hot wire probes were used to measure the velocity and turbulence intensity of the fuel flow. The measurements were obtained as close to the fuel release location as possible at predetermined nodes. Adequate quantitative characterization of the fuel release via the hot wire probe assembly allows the fuel boundary conditions to be used in modeling efforts. The fuel velocity distribution presented in Figure 6 was duplicated in the Vulcan simulation and the actual velocities were scaled to match the overall mass flow rate (0.0093 kg/sec).

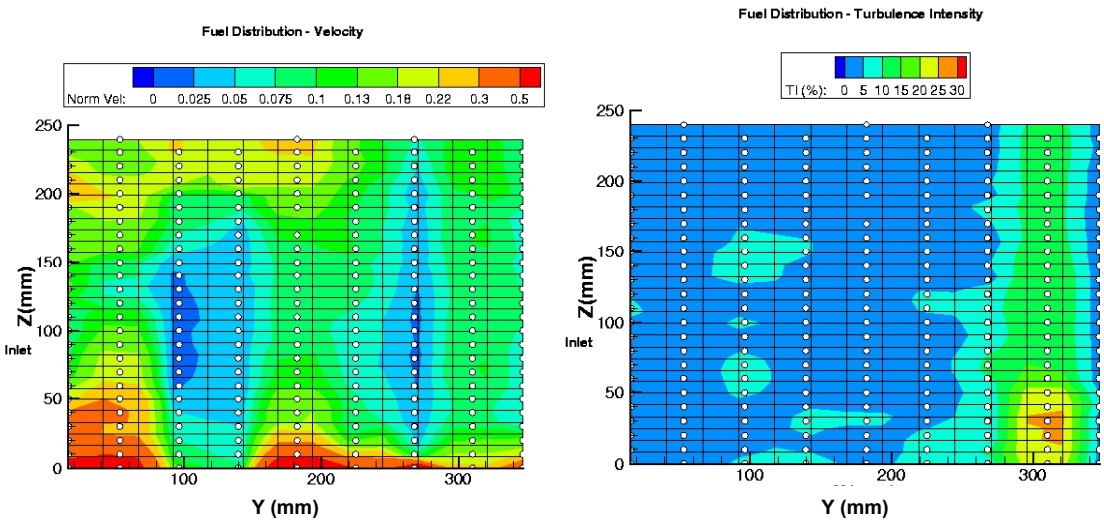


**Figure 6 – Fuel Velocity and Turbulence Intensity Distribution**

For the simulations where uniform flow conditions are assumed at the fuel inlet, the corresponding average velocity is 0.1705 m/s. The average turbulent kinetic energy value was calculated assuming turbulent isotropic flow using a value of 5% for the turbulence intensity.

### 5.3 Outlet

At the outlet of the dry bay simulator, a constant pressure condition was specified using a pressure of 95,151 Pa as measured in the experiment.

### 5.4 Walls

Along the surface of the dry bay simulator, a no-slip wall was specified in the simulation with an initial temperature of 297 K, which corresponds to ambient temperature measured in the experiment. The increase in wall temperature due to the fire was modeled using properties of titanium. A layer of insulation material was also included in the model next to the top wall and two side walls of the dry bay. Surface roughness was not included along any of the walls.

# 6. Simulation Matrix

Simulations were performed using the Vulcan fire field model to assess the sensitivity of the Vulcan solution to the boundary conditions and grid resolution. The first simulation utilized uniform boundary conditions for both the air and fuel inlets. After which, it was determined that the boundary conditions were not uniform and a thorough characterization of the boundary conditions in the experimental test fixture was performed. A simulation of the best estimate of the actual boundary conditions, as determined from the experimental characterization, was run (referred to as non-uniform air, non-uniform fuel). To provide an assessment of the impact of air and fuel boundary conditions on the fire environment, simulations with either the best estimate (non-uniform) or uniform boundary conditions for air and fuel were conducted. In addition, the sensitivity of the solution to grid size was evaluated by comparing two different grid solutions. The simulation matrix is summarized in Table 1.

| | Mesh | Mesh Size | Air Dist. | Fuel Dist. |
|---|---|---|---|---|
| 1 | Fine | 332 k | uniform | uniform |
| 2 | Fine | 332 k | non-uniform | non-uniform |
| 3 | Medium | 219 k | non-uniform | non-uniform |
| 4 | Fine | 332 k | uniform | non-uniform |
| 5 | Fine | 332 k | non-unifom | uniform |

**Table 1. Summary of Simulation Studies**

# 7. Results

Vulcan results were compared to the experimental temperature and heat flux data from the dry bay fire simulator. The Vulcan simulations were run until a steady state solution was obtained. In addition, the sensitivity of the model results to boundary conditions and grid resolution are investigated as outlined in Table 1. The utility of the Vulcan fire model in predicting the thermal hazard posed by a sustained pool fire is assessed.

## 7.1 VULCAN Predictions and Experimental Comparisons

Figure 7 shows a temperature contour plot along the centerline of the dry bay and Figure 8 shows a heat flux contour plot along the sidewall of the dry bay predicted by Vulcan. In the numerical simulation, both the air inlet and the fuel inlet were specified using a velocity distribution based on experimentally measured values which corresponds to Case #2 in Table 1. The colored dots overlaid on the plots represent the measured temperature and heat flux values from one experiment.

In Figure 7, thermocouple temperatures within the test fixture ranged from ambient to 1300 K. Typically a temperature greater than 800 K is indicative of an actively burning region. The Vulcan gas temperatures are similar to the experimental thermocouple values with the Vulcan prediction showing a slightly higher (100-200 K) peak temperature value. It is acknowledged that due to several mechanisms, including radiative transport and thermal inertia (referred to as thermocouple lag), the temperature measured is not, in general, equal to the local gas temperature [9]. This effect can result in a thermocouple reading that is either higher or lower depending on the position of the thermocouple relative to the fire. The temperature plot also shows a burning region surrounding the air stream and a large re-circulation region near the lower rear portion of the dry bay. Due the coarseness of the measurement grid, the thermocouples did not resolve the thin flame region surrounding the air stream and the higher temperature region near the air inlet.

The Vulcan prediction also shows a cold layer of gas along the top portion of the dry bay due to the ambient air stream from the inlet, whereas, the experimental data (Figure 7) show a slight increase in temperature in this region. This temperature difference seems to support experimental observations that an unsteady fire developed in the dry bay which allowed hot gases to enter into the upper region of the dry bay, resulting in higher thermocouple values. The time-averaged (RANS) flow equations employed in Vulcan have difficulty resolving large fluctuating transients which may account for the discrepancy between the predictions and measurements at the top of the duct.

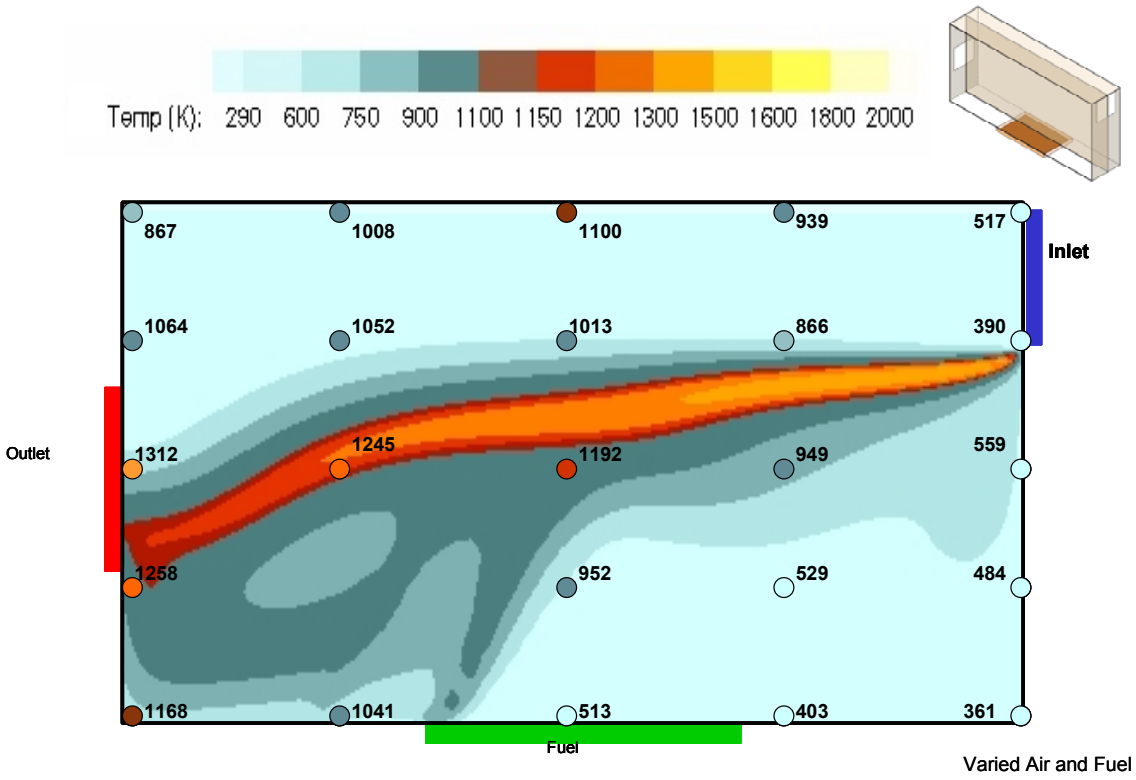


**Figure 7 – Predicted Gas Temperatures and Thermocouple Values**

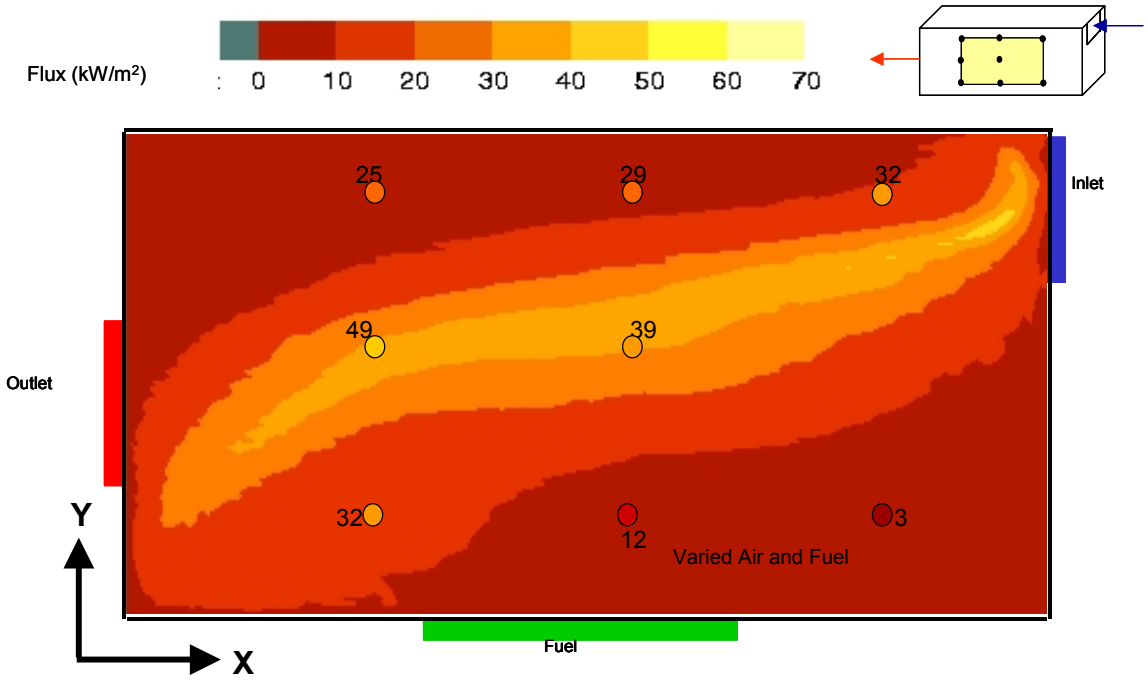


**Figure 8 – Predicted Heat Flux Distribution and Measured Values**

At the exit of the duct, the flow enters into a mixing chamber. Based upon a thermocouple measurement in the mixing chamber (not shown) and the Vulcan prediction, a considerable amount of burning occurred in the mixing chamber.

The peak heat flux and the average heat flux of a fire environment are the most important metrics in the assessment of the thermal hazard of a dry bay fire. Heat flux measurements, which represent the integrated affect of the fire on the system, were recorded up to 49 $kW/m^2$ as shown in Figure 8. There were 9 heat flux gauges in the experiment; however, one gauge failed during the experiment. The average heat flux of the eight measurements is 28 $kW/m^2$. The experimental heat flux values were obtained by averaging over the time interval when the wall temperature of the heat flux gauge with the highest value (i.e., 49 $kW/m^2$) was between 346 K-352 K. This wall temperature range was chosen because it corresponded to a time when the thermocouple measurement reached a steady state value [1]. As expected, regions of high heat flux correspond to areas of increased temperature in the dry bay. The Vulcan heat flux predictions (Figure 8) at the measurement locations are similar but generally lower than the corresponding experimental values. Vulcan also predicts a peak heat flux of 44 $kW/m^2$ and an average heat flux of 12.3 $kW/m^2$ based on nine heat flux values at the measurement locations. The heat flux values were also obtained at a time in the simulation when the wall temperature reached 350 K. The predicted peak heat flux shows a 10% difference with the experimental value, while the average heat flux value shows a 56% difference due to the unsteady fire and the coarseness of the experimental data. The difference in peak heat flux approaches the order of the experimental uncertainty (replicate variability) and probably isn't meaningful; however, the difference in the average heat flux is well above the experimental uncertainty. Again, this difference could be attributed to the unsteady flow features that somewhat broadened the fire over what is predicted by Vulcan and the coarseness of the measurement grid.

The temperature and heat flux trends are also consistent with the video record. The images captured by the camera below the inlet showed the burning occurring overhead and towards the rear of the fixture. The fuel pan is clearly visible throughout the majority of the video indicating that burning is not occurring between the window where the camera is positioned and the end of the fuel pan. The video showed intermittent impingement of the flames on the inlet plane near the window where the cameras were positioned. This movement of flame suggests that an unsteady fire did develop inside the dry bay simulator, even though the intention of this experiment was to produce a steady

fire for comparison to steady numerical predictions. Turbulence models that capture unsteady flow features, as well as buoyancy induced turbulent effects, are under development [10]. It is anticipated that the use of these models will improve the present comparisons for heat flux loads.

## 7.2 Sensitivity Calculations

Figure 9 shows temperature contour plots along the centerline of the dry bay and heat flux contour plots along the sidewall of the dry bay for the medium and fine grid solutions. The medium mesh solution is compared to the fine mesh solution for the case where both the air inlet and the fuel inlet were specified using a velocity distribution based on experimentally measured values (non-uniform air and non-uniform fuel). The temperature contour plots show good agreement with slight differences in the burning region pattern. The heat flux plots also show good agreement with only a 2% difference in peak heat flux value and 0.8% difference in average heat flux between the fine mesh and medium mesh results. Overall, the fine mesh and medium mesh solutions adequately capture the burning regions of the fire in the dry bay. This comparison provides an indication of the level of grid convergence for the fine mesh solution and the amount of numerical error in the solution relative to the uncertainty (+/-5%) in the experimental measurement.

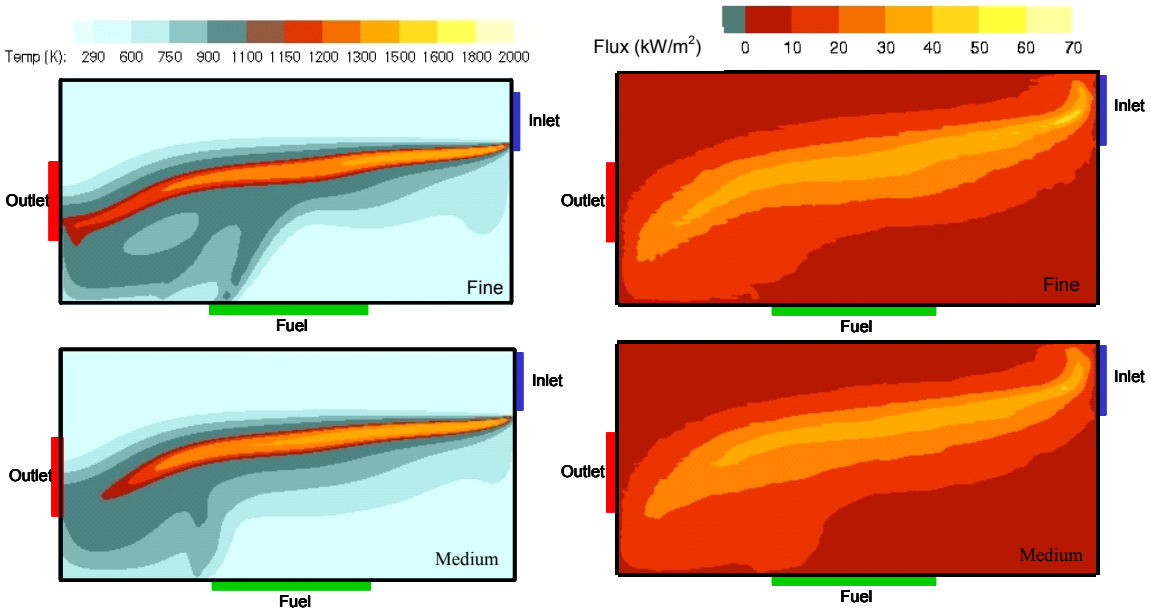


**Figure 9 – Solution Sensitivity to Grid Size**

The sensitivity of the Vulcan solution to different combinations of uniform and non-uniform inlet conditions was investigated. Figure 10 and Figure 11 show temperature contour plots and heat flux contour plots, respectively, of the Vulcan predictions for the variations in boundary conditions studied. It is important to understand the impact of air and fuel inlet conditions on the fire environment since live fire tests involve a variety of scenarios, all of which need to be extinguished.

The temperature contour plots in Figure 10 show similar patterns with a long thin burning region around the air inlet and a re-circulation region in the lower rear portion of the dry bay. In the two cases where a non-uniform air inlet was specified, the gas temperatures are about 200 K higher than the uniform air inlet cases. The heat flux contour plots in Figure 11 also show similar heat flux patterns with the largest differences due to the air inlet conditions. The peak heat flux values are 10-20 kW/m$^2$ higher when a non-uniform air inlet is specified. Overall, the distribution of fuel inlet velocity did not significantly affect the predicted temperature and heat flux values for the cases examined.

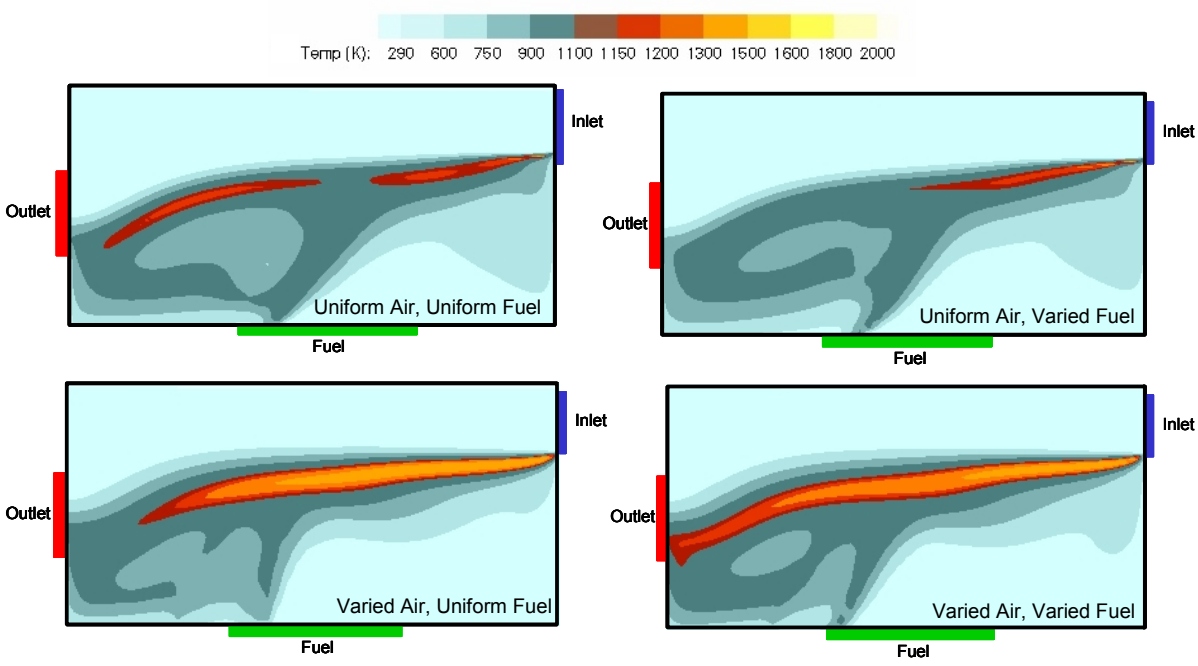


**Figure 10 – Predicted Temperature Distribution for Various Inlet Conditions**

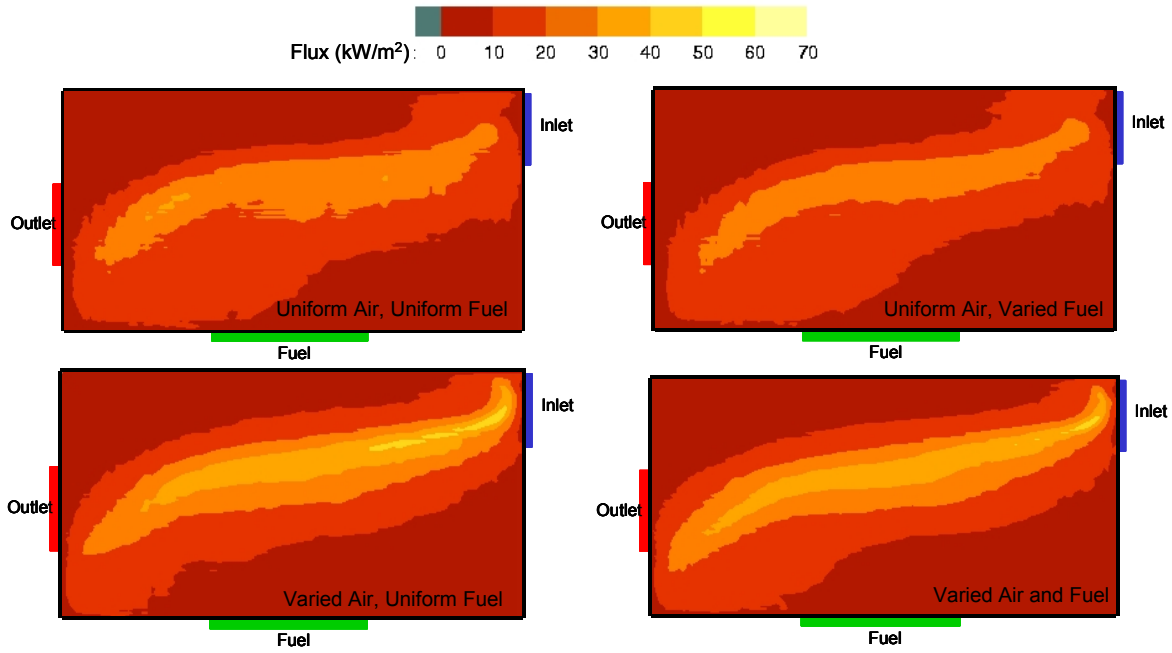


**Figure 11 – Predicted Heat Flux Distribution for Various Inlet Conditions**

Table 2 summarizes the average heat flux error and the peak heat flux error between the predictions and the experimental data for all five cases shown in Table 1. The average heat flux error values are very similar while the peak heat flux error values vary significantly. Case 1 and Case 4 (both uniform air boundary conditions) result in slightly higher average error values and much higher peak error values. Case 2, Case 3, and Case 5 compare well to the experimental peak heat flux value. Recall that Case 2 and Case 3 provide the best estimate of the boundary conditions using a fine mesh and a medium mesh, respectively. The difference in error values due to mesh size (0.8% average heat flux and 2% peak heat flux) are much less than the maximum difference in error values due to the boundary conditions (3% average heat flux and 37% peak heat flux). Again, this gives an indication that the level of grid convergence is adequate for this problem.

| Case # | 1 | 2 | 3 | 4 | 5 |
|---|---|---|---|---|---|
| Average Heat Flux Error | 57% | 56% | 56% | 59% | 56% |
| Peak Heat Flux Error | 33% | 10% | 12% | 41% | 4% |

**Table 2. Heat Flux Error Summary**

# 8. Conclusions

The utility of using the Vulcan fire field model in dry bay fire scenarios has been assessed. A description of a dry bay fire test fixture, fuel and air inlet boundary conditions, and an experimental data set are included in the report. Vulcan temperature and heat flux predictions were compared to the experimental data from the dry bay simulator.

In general, the Vulcan temperature range and peak temperatures showed good agreement with the experimental data. However, at the specific measurement locations, differences were observed between the predicted gas temperatures and the experimental thermocouple values. These differences were due to the known lag time of the thermocouple measurement and the coarseness of the measurement grid. Also, thermocouples respond to the local radiative heat flux and can be higher or lower depending on the position of the fire relative to the thermocouple. In addition, an unsteady fire developed in the experiment, which caused flames to intermittently move into the upper portion of the dry bay. As a result, the thermocouples located in the cold air stream region registered higher temperatures.

The average heat flux and the peak heat flux of a fire environment are the most important metrics in the assessment of the thermal hazard of a dry bay fire. The predicted peak heat flux value showed good agreement with the experimental data, while the average values differed due to the unsteady fire in the experiment and the coarseness of the measurement grid. This difference highlights the need to fully characterize the fire environment with adequate measurement coverage, as well as, the limitations in the current turbulence model formulation. More complete treatments are under development [10].

A sensitivity study was also performed for the purpose of assessing the impact of boundary condition details and grid resolution on the predicted fire environment. For the flow rates and configuration studied, the fire environment was not significantly affected by changes in the distribution of flow at the fuel boundary condition; however, larger differences occurred when the distribution of flow at the air boundary condition was changed. Good agreement in results was obtained for two different grid sizes.

The Vulcan fire field model has shown the capability to predict the thermal hazard from a sustained pool fire within a dry bay compartment of an aircraft. However, there are several suggestions for improving the experimental set up in order to obtain higher

quality data for validation of the fire code so that a final assessment of the usefulness of the code can be made. These improvements are as follows:

1) Because of the coarseness of the experimental data set, the dry bay fire was not fully characterized and direct comparisons with the Vulcan predictions were incomplete. Better spatial resolution of dry bay fire can be obtained using additional conventional and advanced diagnostics.
2) The observed movement of flame during the experiment suggests that an unsteady fire developed inside the dry bay simulator beyond the normal turbulent fluctuations. While such unsteadiness may occur in actual application, an attempt was made to design a steady fire experiment for the purposes of code validation. The final experimental design, however, included a high degree of left/right symmetry, which tends to promote large-scale unsteadiness through mode bifurcation. Future studies should employ deliberate asymmetry, such as moving the air inlet to the corner of the dry bay, in order to achieve a steady fire scenario.
3) The quality of any experimental data set is determined from the error and uncertainty estimations. Due to lack of resources, it was not possible to run multiple tests for the final configuration used in this study to determine a more accurate measurement uncertainty.

## References


1. Gill, W., Suo-Anttila, J., Black, A., Tieszen, S., and Gritzo, L., "Experimental Characterization of a Dry Bay Fire Environment," Sandia report SAND2003-0625J, to be published.
2. Lopez, A., Gritzo, L. and Gill, W. "Dry Bay Fire Simulations for Simplified Geometries," A letter report to Dr. Frank Mello, OSD/LFT&E (March 1999).
3. Patankar, S.V., and Spalding, D.B., *Int. J. Heat Mass Transfer*, 15:1787, 1972.
4. Magnussen, B.F., Hjertager, B.H., Olsen, J.G., and Bhaduri, D., "Effects of Turbulent Structure and Local Concentrations on Soot Formation and Combustion in C2H2 Diffusion Flames." *The Seventeenth Symposium (International) on Combustion*, The Combustion Institute, Pittsburgh, pp. 1383-1393, 1979.
5. Magnussen, B.F., "The Eddy Dissipation Concept," Proceedings of the Eleventh Task Leaders Meeting, IEA Working Group on Conservation in Combustion, Lund, Sweden, 1989.
6. Magnussen, Particulate Carbon Formation During Combustion, Plenum Publishing Corporation, 1981.
7. Tesner, P.A., Snegiriova, T.D., and Knorre, V.G., "Kinetics of Dispersed Carbon Formation," Combustion and Flame, vol. 17, pp. 253-271, 1971.
8. Shah, N.G., *"The Computation of Radiation Heat Transfer,"* Ph.D. Thesis, University of London, Faculty of Engineering, 1979.
9. Gritzo, L.A., Gill, W., and Keltner, N., "Thermal Measurements to Characterize Large Pool Fires," Proceedings of the 41st International Instrumentation Symposium, Denver, CO, May 7-11, 1995.
10. Rouson, D., Tieszen, S. R., and Evans, G., "Modeling convection heat transfer and turbulence with fire applications: a high temperature vertical plate and methane fire," Proceedings of the 2002 Summer Program, Center for Turbulence Research, Stanford, CA. (in press).

## Distribution

Aerospace Survivability Flight
46OG/OGM/OL-AC
Bldg. 1661B, Area B
Attn.: Dr. Peter Disimile
WPAFB, OH 45433-7605

Mr. Andy Pascal
P.O. Box 244
Cedar Crest, NM 87008

Aerospace Survivability Flight
Attn.: Mr. Marty Lentz
46OG/OGM/OL-AC
Bldg. 1661B, Area B
WPAFB, OH 45433-7605

Aerospace Survivability Flight
46OG/OGM/OL-AC
Attn.: Mr. Robert Crosby
Bldg. 1661B, Area B
WPAFB, OH 45433-7605

NAWCWPNS
Attn.: Mr. Leo Budd
Code 418300D
1 Administration Circle
China Lake, CA 93555-6100

Office of the Secretary of Defense, DDOT/LFT&E
Attn.: Mr. Thomas Christie
Deputy Director, Operational Test and Evaluation
1700 Defense Pentagon
Washington, DC 20301-1700

Office of the Secretary of Defense, DOT&E/LFT&E
Attn.: Robert A. Wojciechowski
The Pentagon, Room 1C730
1700 Defense Pentagon
Washington, DC 20301-1700

Naval Air Systems Command, AIR 4.3.5.1
Aircraft Fire Protection
Attn.: Lawrence Ash
48110 Shaw Rd., Bldg. 2187, Suite 3380-D4
Patuxent River, MD 20670-5304

JTCG/AS Central Office
Attn.: Mr. Joseph Jolley
Director, Vulnerability Reduction Subgroup
Crystal Square Four, Suite 1103
1213 Jefferson Davis Hwy.
Arlington, VA 22202-4304

The Boeing Company – Phantom Works
Attn.: Glenn Harper
Mailcode S106 7075
PO Box 516
St. Louis, MO 63166-0516

Air Force Aeronautical Systems Center
Attn: Hugh Griffis
Bldg. 11a, Room 101H
1970 Monahan Way
WPAFB, OH 45433-7208

**Internal Distribution**

| | | | |
|---|---|---|---|
| 1 | MS 0841 | 09100 | T.C. Bickel |
| 1 | MS 0324 | 09130 | J. L. Moya |
| 1 | MS 0828 | 09133 | M. Pilch |
| 5 | MS 0828 | 09133 | A. R. Black |
| 2 | MS 0821 | 09132 | L. A. Gritzo |
| 1 | MS 1135 | 09132 | A. Brown |
| 1 | MS 1135 | 09132 | V. Figueroa |
| 1 | MS 0836 | 09132 | J. M. Nelsen |
| 5 | MS 0836 | 09132 | W. Gill |
| 1 | MS 1135 | 09132 | V. F. Nicolette |
| 5 | MS 1135 | 09132 | J. M. Suo-Anttila |
| 4 | MS 1135 | 09132 | S. R. Tieszen |
| 1 | MS 0836 | 09141 | S. P. Domino |
| 1 | MS 0718 | 06141 | C. Lopez |
| 1 | MS 9018 | 08945-1 | Central Technical Files |
| 2 | MS 0899 | 09616 | Technical Library |